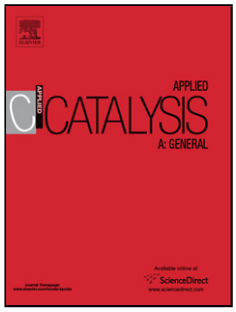

Title: Improving 1,3-butadiene yield by Cs promotion in ethanol conversion

Authors: Pratap T. Patil, Dapeng Liu, Yan Liu, Jie Chang, Armando Borgna

PII: S0926-860X(17)30233-8
DOI: http://dx.doi.org/doi:10.1016/j.apcata.2017.05.025
Reference: APCATA 16247

To appear in: *Applied Catalysis A: General*

Received date: 18-1-2017
Revised date: 14-5-2017
Accepted date: 24-5-2017

Please cite this article as: Pratap T.Patil, Dapeng Liu, Yan Liu, Jie Chang, Armando Borgna, Improving 1,3-butadiene yield by Cs promotion in ethanol conversion, Applied Catalysis A, Generalhttp://dx.doi.org/10.1016/j.apcata.2017.05.025

Improving 1,3-butadiene yield by Cs promotion in ethanol conversion

Pratap T. Patil[#], Dapeng Liu[#], Yan Liu, Jie Chang, Armando Borgna*

*Institute of Chemical and Engineering Sciences (ICES), A*STAR (Agency for Science, Technology and Research), 1 Pesek Road, Jurong Island, Singapore 627833, Singapore*

[#] These authors contributed equally to this work

**Corresponding author, E-mail address: armando_borgna@ices.a-star.edu.sg*

Tel: (+65) 67963802, Fax: (+65) 6316-6182

Graphical Abstract

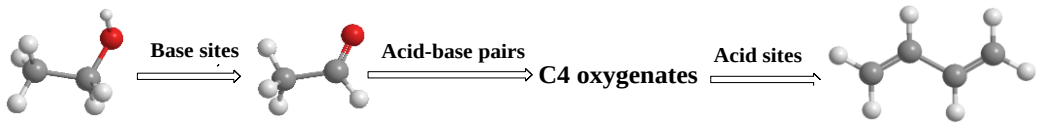

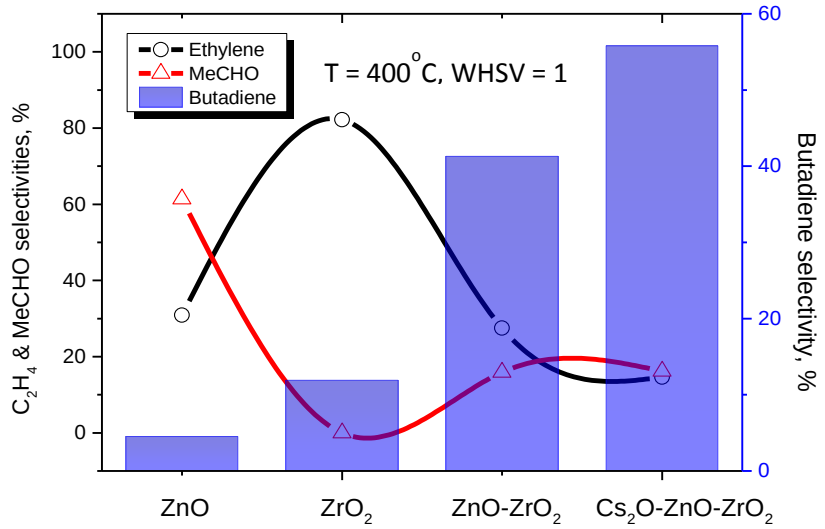

Highlights

- Alkali promotion inhibits ethanol dehydration to ethylene
- Only Cs promotion provides the appropriate balance of acid-base pairs to carry out the condensation step effectively
- Cs is the most promising alkali-metal promoter.
- A single-pass 1,3-butadiene yield of 54.6 % can be obtained over $0.5Cs_2O$-1ZnO-$5ZrO_2/SiO_2$ Catalyst.

1 Introduction

Due to growing concerns on depletion of petroleum resources and climate change resulting from the consumption of petrochemicals and fuels, last few decades have witnessed a renewed interest in converting biomass-derived feedstocks into value-added chemicals [1]. Currently bio-ethanol is being produced abundantly through biomass fermentation and its increased availability opens up new opportunities for the synthesis of renewable bulk chemicals [2, 3]. Therefore, it became highly attractive to develop heterogeneous catalytic systems to effectively convert ethanol to 1,3-butadiene (BDE), one of the most important chemical intermediates in the production of various polymers (e.g. styrene-butadiene rubber, car tiers and plastics) [3, 4]. Currently BDE is obtained as a by-product during steam cracking of naphtha to make ethylene, where an expensive separation by extractive distillation is required [5]. Although the current low oil price strongly benefit this route for BDE production, the trend of shifting to lighter feedstocks such as shale gas will significantly decrease the BDE yield, thus making on-purpose BDE even more attractive and necessary.

Catalytic production of BDE from ethanol can be achieved through either one-step process developed by Lebedev or a two-step process based on Ostromislensky reaction, which were already known since early twentieth century. However both processes were stopped after 1960s due to the lack of competitiveness with petrochemical-based routes [6]. Early investigation by Union Carbide revealed that tantalum oxide and zirconium oxide gave decent selectivity toward butadiene during ethanol conversion. Mixed oxide systems, including $MgO\text{-}SiO_2$, $ZnO\text{-}Al_2O_3$, $ZrO_2\text{-}SiO_2$ and $Zn_xZr_yO_z$ were and still are widely investigated for the Lebedev synthesis [7-13]. Recent progress on catalyst development for converting ethanol to BDE in one or two-steps has

been reviewed by Pomalaza et al. [14], being the optimum balance between basic, acid and redox sites crucial for achieving high BDE selectivity using a single catalyst. For $MgO\text{-}SiO_2$ system, the Mg/Si ratio, the synthesis method as well as the effect of dopands were found to be critical parameters affecting BDE production [7]. Both metallic Cu and Ag have been identified as effective dopants, promoting lower temperature dehydrogenation [7, 9, 10]. The investigation of structure-activity relationship indicated that the importance of fine tuning the distribution of acid-base sites and their proximity due to a cascade reaction involved in the case of $MgO\text{-}SiO_2$ catalysts [11]. In another study, sol-gel synthesized $ZrO_2\text{-}SiO_2$ catalysts showed good performance in ethanol-acetaldehyde reaction since the addition of ZrO_2 creates new Lewis acid sites, promoting the aldol condensation step despite its low dehydration capability [12]. Jones and co-workers reported a considerable selectivity towards BDE (39 %) at moderate ethanol conversion (46 %) over mesoporous SiO_2 supported $ZnO\text{-}ZrO_2$ catalysts, where the addition of copper can increase the BDE selectivity further to 67 % [15, 16]. The importance of the synergetic effect between ZnO and ZrO_2 to enhance the aldol condensation rate and provide additional Lewis acid sites was also reported by Larina et al. [17]. By adjusting surface acid-base properties of $Zn_xZr_yO_z$ mixed oxide with Na ions, the catalyst deactivation was significantly decreased, while BDE selectivity was improved [13].

Although widely investigated, the reaction mechanism from ethanol to BDE is still a matter of debate. It is generally accepted that efficient production of BDE requires several critical steps displayed in Scheme 1 [15]. The first step is the ethanol dehydrogenation for producing acetaldehyde, followed by the aldol condensation between two acetaldehyde molecules yielding acetaldol which is subsequently dehydrated to crotonadehyde. Then, the carbonyl group of

crotonaldehyde can be reduced to the hydroxyl of ethanol by Meerwein-Ponndorf-Verley (MPV) reduction, and the further dehydration of crotyl alcohol leads to butadiene [18]. Alternatively, MPV reduction may happen between acetaldol and ethanol, thus forming 1,3-butanediol, which can be dehydrated to the target product, BDE. It is important to stress that reaction intermediates such as 1,3-butanediol, crotonaldehyde, and crotyl alcohol, proposed base on literature, were not detected under our reaction conditions. In addition, Scheme 1 also includes a reaction pathway to account for the production of light olefins. Indeed, ethylene is always produced, sometimes in large quantities, via direct or indirect dehydration of ethanol, while C_3-C_4 olefins are formed in rather small quantities, probably via an acid catalyzed mechanism similar to that of Ethanol-to-Olefins (ETO) process.

Abstract

Gas phase conversion of ethanol into butadiene was studied over silica-supported ZnO, ZrO_2 and ZnO-ZrO_2 catalysts in a fixed-bed reactor. Surface active sites were characterised using a variety of techniques including temperature-programmed desorption (TPD) of NH_3 and CO_2 as well as Fourier transform infrared (FTIR) spectroscopy of adsorbed pyridine. An increased concentration of acid and base sites was found in the following order: ZnO < ZrO_2 < ZnO-ZrO_2 s. In addition, new acid and base sites were generated when alkaline metal promoters were introduced. The typical products observed for all these catalysts include acetaldehyde, butadiene, ethylene, butenes, diethyl ether and C_4 oxygenates. As compared to single oxide supported catalysts, a remarkable acid-base synergetic effect was observed on the binary oxides supported catalysts with or without alkali metal modification. The improved catalytic activity and higher selectivity can be attributed to the right balance between acid and base sites, minimizing dehydration toward ethylene while

promoting dehydrogenation toward acetaldehyde as well as the existence acid-base pairs with the appropriate configuration and strength which accelerates aldol condensation and Meerwein-Ponndorf-Verley (MPV) reduction reactions efficiently.

In this contribution, we report on the influence of alkali metal promoters on the selective ethanol conversion into BDE over SiO_2 supported Zn-Zr catalysts. Special emphasis is placed on the role of acid-base centers on the improvement of the catalytic performance of $ZnO\text{-}ZrO_2/SiO_2$ catalysts.

2 Experimental

2.1 Catalyst preparation and characterisation

Supported catalysts were prepared by incipient wetness impregnation method with different contents of metal oxides (ZnO: 1 wt%, ZrO_2: 5 wt%) and 0.5 wt% of alkali-promoters (Li_2O, Na_2O, K_2O, Cs_2O) using commercially available fumed silica, zirconium oxynitrate, zinc nitrate, lithium nitrate, sodium nitrate, potassium nitrate, rubidium chloride and cesium nitrate as precursors. For comparison purpose, the catalysts with the same molar loading of alkali-metal were also prepared. Specifically, the molar ratio of Zn/alkali was fixed at 6.9. All catalysts were dried at 110 ^oC overnight and then calcined at 500 ^oC for 4 h before measurements. The resulting supported catalysts are named as $xM_2O\text{-}yZnO\text{-}zZrO_2/SiO_2$ where x, y and z are the loadings of the corresponding oxides and alkali metal promoters (M represents the alkali metals). Powder X-ray diffraction (XRD) patterns of the samples were recorded using a Bruker D8 Advance diffractometer with Ni-filtrated Cu Kα radiation ($\lambda = 1.5406^{\circ}A$) produced by a Cu anode operated at 40 kV and 40mA. N_2 physisorption was carried out at -196 °C on a Micromeritics ASAP 2020 analyser. The samples were degassed at 200 ^oC for 24 h prior adsorption measurements. Temperature-programmed desorption (TPD) of NH_3 was carried out on a Thermo Scientific

TPDRO 1100 apparatus equipped with a thermal conductivity detector (TCD). About a 100 mg sample was activated at 500 ^{o}C for 1 h under argon flow before NH_3 adsorption at 150 ^{o}C for 1 h. After adsorption, the sample was flushed with Ar for 1 h and then the temperature was increased up to 800 °C with a heating rate of 10 ^{o}C/min while the desorption of NH_3 was monitored using TCD. The peak area was correlated with the amount of adsorbed NH_3 based on calibration values obtained from the injection of NH_3 pulses. Base strength was measured by CO_2-TPD in the same system as mentioned above and using a similar procedure in which CO_2 adsorption was carried out at 30 ^{o}C instead of NH_3 adsorption at 150 ^{o}C. Infrared spectroscopy (FT-IR) of adsorbed pyridine was recorded in a BIO-RAD FTS-3000MX IR spectrometer. The catalysts were pressed into self-supporting wafers, which were then inserted in the IR cell. Before pyridine adsorption, the sample was pretreated in vacuum system at 300 °C for 1 h. Then the system was cooled down to room temperature under vacuum and expose to the purified pyridine until saturation was achieved. Spectra were recorded after evacuation for 30 min at increasing temperatures. The background spectrum was recorded under identical conditions without pyridine adsorption and automatically subtracted.

2.2 Activity tests

Catalytic reactions were carried out in a continuous down-flow fixed-bed microreactor under atmospheric pressure. Typically, 0.5 g of the sieved catalyst (mesh size 250 -400 μm) was diluted with equal volume of silicon carbide and packed between two layers of quartz wool in the reactor. The upper portion of the reactor was filled with glass beads serving as preheater and mixer for the reactants. Prior to introducing the feedstock, the catalyst was pretreated in flowing nitrogen (50 mL/min) for 1 h at 400 °C. The reaction temperature was measured by a type K thermocouple located in the catalyst bed and connected by a PID-type temperature controller. Catalytic tests

were performed by injecting ethanol (HPLC grade) with HPLC infusion pump (Agilent 1100 series). 5 % Ar was mixed with He carrier gas as the internal standard, allowing for the calculation of the total molar flow of the gas products by monitoring the Ar peak area in the TCD detector. Ethylene, which is always produced during the reaction and can be detected on both TCD and FID detectors, was employed as bridge compound to calculate the real molar flow rates for each hydrocarbon product. The hydrocarbon products were analyzed with an online gas chromatograph (Shimadzu) equipped with a Flame Ionization Detector (FID), using a PONA capillary column (150 m × 0.25 mm ×1.0 μm). During all catalytic tests, the weight hourly space velocity (WHSV) was fixed at 1 h^{-1} and the reaction temperature at 400 °C, except in the temperature optimization experiments. All the reaction data were collected after 3 h of time-on-stream. Ethanol conversion (X%), selectivity of product i (S_i) and yield of product i (Y_i) were calculated based on equations (1)-(3), where $F_{EtOH,\ in}$ and $F_{EtOH,\ out}$ refer to molar flow of ethanol in and out of the reactor, respectively; Pi represents the moles of a specific product i and n is the total number of products:

$$X(\%) = \frac{F_{EtOH}^{in} - F_{EtOH}^{out}}{F_{EtOH}^{in}} * 100 \qquad (1)$$

$$S_i(\%) = \frac{P_i}{\sum_{i=1}^{n} P_i} * 100 \qquad (2)$$

$$Y_i(\%) = S_i(\%) * X(\%) / 100 \qquad (3)$$

3 Results and discussion

3.1 Catalyst characterisation

The textural of the catalysts were analyzed using N_2 adsorption. The BET surface area of the supported catalysts (Table 1) decreases with increasing the loading of active components due to

the deposition of oxide species on the silica surface. The XRD pattern (not shown) only reveals the amorphous phase of the carrier without showing any reflection corresponding to ZnO, ZrO_2 or Cs_2O crystallites, indicating a good dispersion of these oxide particles on the high surface silica.

NH_3-TPD was carried out to determine the acid amount and strength of the acid sites of the catalysts. The corresponding profiles are shown in Fig. 1. The total acidity of the catalysts was calculated as the sum of the weak and moderate acid sites, obtained by curve fitting using a Gaussian deconvolution procedure.

As shown in Fig. 1, no NH_3 adsorption is observed on SiO_2 and ZnO/SiO_2, indicating either the absence of acid sites or the existence of very weak ones. Clearly, acid sites are generated upon ZrO_2 introduction. The NH_3-TPD profiles show a broad desorption signal between 200 °C to 350 °C indicating the presence of acid sites of weak to moderate strength, but the absence of strong acid sites. The existence of such a moderate acid sites is reasonable since these oxides lack of framework hydroxyl groups as in the case of zeolitic materials [19]. For the samples containing both ZnO and ZrO_2, the peak shifts to higher temperature, indicating that the acid strength is increased as compared to the ZrO_2 supported sample. Both the concentrations of weak and moderate acid sites increase, leading to an increase in total acid density. After doping with Cs_2O, a slight decrease of the acidity reflects the partial neutralization of acid sites by the presence of Cs_2O.

FT-IR spectra of adsorbed pyridine were measured after desorption at 200 °C on the catalyst series to removed physisorbed pyridine and the concentration of acid sites was calculated by integrating the intensity of the corresponding IR bands [20]. As shown in Fig. 2, all the samples

presented strong adsorption bands at lower frequencies, 1446-1452 cm^{-1}, which is attributed to the adsorption of pyridine on Lewis (L) acid sites. While the band around 1490 cm^{-1} is related to the vibrations of pyridine co-adsorbed on Brønsted (B) and Lewis acid sites, the weak band at 1545 cm^{-1}, which is caused by formation of pyridinium ions, indicates the presence of B acid sites. Brønsted acid sites are clearly observed only on ZrO_2 catalyst and marginally observed on the Cs_2O modified catalysts, while Brønsted sites are absent over ZnO and ZnO-ZrO_2 catalysts. For the Lewis acid sites, the position of the band is related to the strength of Lewis acid sites. The weak acid strength of the support is consistent with the lower frequency at 1447 cm^{-1}. The presence of weak acid sites is also observed for ZrO_2-based catalysts, while a higher frequency at 1452 cm^{-1} over ZnO catalyst indicates the relatively higher acid strength. Pyridine adsorption also shows that ZrO_2 generates both B and L acid sites and the presence of ZnO removes B acidity. Addition of Cs_2O decreases by roughly 55% the L acid centres but slightly increases B acidity. The concentrations of B and L acid sites at 200 ^oC desorption is summarized in Table 2. The concentration of L acid sites of the samples follows the sequence: SiO_2 < 1ZnO/SiO_2 < 5ZrO/SiO_2< 0.5Cs_2O-1ZnO-5ZrO_2/SiO_2 < 1ZnO-5ZrO_2/SiO_2.

The results of CO_2-TPD are plotted in Fig. 3. Similar to NH_3-TPD, the temperature of desorption can be co-related to the relative base strength of the catalysts. A desorption peak at a lower temperature (~100 ^oC) was observed for all the materials, suggesting the existence of weak base sites. However, upon addition of Cs_2O, an additional desorption peak at ~230 ^oC is observed, indicating the formation of stronger base sites. The concentration of the base sites increases in the following sequence: SiO_2 (1.9 µmol*g^{-1}) < 1ZnO/SiO_2 (2.7 µmol*g^{-1}) < 5ZrO_2/SiO_2 (6.5 µmol*g^{-1}) < 1ZnO-5ZrO_2/SiO_2 (6.8 µmol*g^{-1}) < 0.5Cs_2O-1ZnO-5ZrO_2/SiO_2 (9.7 µmol*g^{-1}).

Based on scanning electron microscopy (Fig. 4), the morphology of the samples is irregular and no crystalline particles are present. However, after loading of metal oxide(s), particle agglomeration happens, particularly for the catalyst containing the three oxides. Since co-impregnation was used to prepare these catalysts, a good dispersion of supported oxide is expected. The good dispersion of surface active components (Cs_2O, ZnO and ZrO_2) is consistent with the XRD measurements.

3.2 Catalytic Activity

The catalytic results of SiO_2 supported Zn and Zr oxides are summarised in Table 3. The bare support exhibits a quite low ethanol conversion (~17 %) without any BDE production, suggesting the absence of suitable active sites. However, ethanol dehydrogenation to acetaldehyde is readily achieved due to the presence of a relatively small amount of weak Lewis acid sites as indicated by pyridine results. The introduction of Zn and Zr oxides leads to a significant increase in ethanol conversion as well as a substantial change in selectivity. Clearly, the selectivity towards ethylene and BDE increases, while the selectivity towards acetaldehyde is significantly decreased. Relatively small amounts of other products are also observed over Zn and Zr oxide catalysts, including light olefins (propylene and butenes), oxygenates (diethyl ether, crotonaldehyde, 1-butanol, ethyl acetate) and few unidentified compounds. No higher hydrocarbons ($\geq C_6$) are observed probably because the acid strength of these catalysts is relatively weak. However, the selectivity pattern of $1ZnO/SiO_2$ and $5ZrO_2/SiO_2$ catalysts is clearly different. While $1ZnO/SiO_2$ exhibits a superior performance for dehydrogenating ethanol to acetaldehyde (yield ~45 %) and a relatively low dehydration activity (yield ~23 %), the Zr-based catalyst produces mainly ethylene (yield ~82 %). In both cases, a marginal production of BDE is observed (BDE selectivity < 10 %), clearly indicating that the condensation pathway does not occur efficiently. Particularly, in the case

of $5ZrO_2/SiO_2$, the low BDE selectivity might be due to the lack of Zr-O-Si bond formation due to the preparation procedure [19].

A significant increase in BDE yield is observed when a $ZnO\text{-}ZrO_2$ catalyst is employed, yielding a BDE selectivity of 41.3 % at 95.3 % ethanol conversion. At the same time, the selectivity toward the two primary products decreases to 27.5 % and 15.9 % for ethylene and acetaldehyde, respectively. This is in well agreement with recent results by Jones and co-workers [14], who reported similar selectivity values (45.8 % BDE, 30.7 % ethylene and 13.8 % acetaldehyde) over mesoporous silica supported Zn-Zr catalysts.

The influence of reaction temperature on catalytic performance was studied using the $1ZnO\text{-}5ZrO_2$ catalyst in the range of 325-500 ^oC. As shown in Fig. 5, the conversion of ethanol increases gradually with the temperature, from around 88 % at 325 ^oC to 100 % at temperatures $\geq$ 450 ^oC. Butadiene selectivity shows a volcano trend, with an optimal value around 45 % at 400 ^oC. At relatively lower temperatures, especially at 325 ^oC, the formation of oxygenates such as diethyl ether and acetaldehyde (23 % and 18 %, respectively) hinders the catalytic performance. At temperatures higher than 400 ^oC, ethylene becomes the major product progressively, reaching 43 % ethylene at 500 ^oC. The subtle balance between the rates of dehydrogenation, aldol condensation, MPV and dehydration can be well maintained at the optimal temperature of 400 ^oC.

The effect of alkali metal oxides on the catalytic performance was further examined by modifying the Zn-Zr catalysts with alkali metals. The catalytic results are summarized in Table 4. As shown in Table 4a, when the loading of alkali metal oxide is 0.5 wt%, all modified catalysts present higher BDE selectivity except for Li_2O-containing catalyst. The yield of BDE increases in the following order: $0.5Li_2O\text{-}1ZnO\text{-}5ZrO_2/SiO_2$ (25.5 %) < $1ZnO\text{-}5ZrO_2/SiO_2$ (39.4 %) < 0.5 K_2O-

1ZnO-5ZrO_2/SiO_2 (41.3 %) < 0.5Na_2O-1ZnO-5ZrO_2/SiO_2 (44.2 %) < 0.5Cs_2O-1ZnO-5ZrO_2/SiO_2 (54.6 %).

However, due to the significant difference in the atomic weight of the alkali metal promoters, their effect was further investigated at the same Zn/M molar ratio (6.9 mol/mol), where M represents the different alkali metals. As shown in Table 4b, the ethanol conversion slightly increases for the Li-promoted sample as compared to the parent Zn-ZrO_2/SiO_2 catalyst, along with a decrease of ethylene and acetaldehyde formation and an increase of propylene selectivity. When the promoters with higher basicity were loaded, the ethanol conversion slightly decreases when Na and K are used as promoter,while higher conversion levels are observed for Rb and Cs. Significant amount of diethyl ether is detected in the case of Na- and K- promoted catalysts, while it is negligible over Rb- and Cs-modified catalysts. Furthermore, the formation of ethylene is inhibited unsurprisingly in the same order with the basicity of the promoters, which is ascribed to the poisoning of acid sites.

BDE yield over Li-promoted catalyst becomes slightly better than than the one observed on the unpromoted catalyst, while Na- and K-modified catalysts exhibit lower BDE selectivity. Only when the basicity of promoters are stronger than potassium, as in the case of Rb and Cs, the yield of BDE increases again, being Cs_2O the most promising one for maximizing the yield of BDE via a synergetic effect of the catalytically active sites.

During BDE synthesis, various products can be formed via dehydrogenation, dehydration, condensation and reduction, heightening the importance of the right balance of surface acid and base sites. On the bare SiO_2 support the catalytic activity for alcohol conversion is quite low due

to the lack of active sites. The introduction of small amount of ZnO increases both dehydrogenation and dehydration rates, being the dehydrogenation path to form acetaldehyde as the dominant one (Table 3). This reflects that the required dehydrogenation step occurs quite efficiently, but the subsequent condensation step to form C_4 oxygenates does not occur significantly due to the lack of suitable active sites. Even though the highest selectivity to ethylene is observed over supported ZrO_2 catalyst, a modest amount of BDE is also formed, which is consistent with previous observations indicating that ZrO_2 promotes the MPV reaction [22, 23]. When ZnO and ZrO_2 are simultaneously present on the catalyst, the concentrations of both acid and base sites increase as compared to the ones on the single oxide supported catalysts, generating acid-base pairs with the right configuration and strength to efficiently promote the condensation of acetaldehyde and significantly increasing the BDE yield, in well agreement with previous reports [14].

It is well known that the rational distribution of various surface active sites is a perquisite to accomplish multiple-step transformations effectively. Regarding site requirement, it is well recognized that dehydration is catalyzed on acid sites while the dehydrogenation occurs on base sites. It was emphasized that strong base sites hardly produce ethoxide intermediates from ethanol dissociation and, therefore, base sites of low and moderate strength are sufficient to promote dehydrogenation [24]. Aldol condensation and MPV are two key reactions for carbon chain growth. For aldol formation, the reaction takes place on acid, base or acid-base catalysts [25-28] wherein a bimolecular surface adsorption and activation is involved in the condensation. Similar active sites are required for the MPV reduction, where alcohols serve as hydrogen donors [22, 29]. However, the resulting selectivity in a complex reaction pathway involving both parallel

and sequential routes as the one displayed in the Scheme 1 strongly depends on the strength and balance of all active sites. In order to achieve high BDE selectivity, the undesired dehydration to ethylene has to be minimized, while the sites promoting dehydrogenation and condensation have to be maximized. Therefore, alkali metals were added to optimize the balance of the active sites and gain more insights into the relationship between reactivity and acid-base properties of the catalysts. The characterization of acid-base properties indicates that while acidity is significantly decreased upon introduction of alkali metals, the concentration of base sites is enhanced substantially. The decrease in acidity upon alkali promotion leads to a beneficial effect, significantly decreasing the undesired formation of ethylene (from ~25% to 10-15%). The changes in the nature and balance of surface active sites obviously increase surface adsorption and key condensation steps of acetaldehyde through inhibiting direct dehydration. However, no straightforward relationship is present between BDE formation and concentrations of acid/base sites for the alkali metal containing catalysts (Fig. 8, bare Zn-Zr catalyst was added as a reference). Although BDE selectivity is maintained, the activity is rather low on lithium-containing catalyst due to lack of acid sites, resulting in lower BDE yield. In addition, though Li efficiently inhibits ethylene formation, the lack of acid-base pairs does not efficiently catalyze the condensation step, resulting in higher acetaldehyde selectivity. As compared to Li, Na and K increase both acid and base sites, leading to higher activity and slightly higher BDE selectivity. As a result, the BDE is much higher than the one observed on Li-promoted catalyst but only marginally better than the unpromoted sample. However, a clear improvement on BDE yield occurs in the presence of Cs. This improvement is clearly associated not only with the increase concentration of both acid and base sites on the Cs-promoted catalyst but also with the generation of base sites with

moderate strength, which are only observed on Cs sample as shown by CO_2-TPD experiments. It should be emphasized that both the aldol condensation and MPV reaction involve two substrates chemically adsorbed on two adjacent active sites. Therefore, a high density of acid-base pairs facilitates the formation of C_4 oxygenates. In general, these results are in good agreement with a recent work published by Da Ros et al. [30] reporting that the promotion with alkali metals results in a decrease of ethanol dehydration whilst increasing the combined BDE and acetaldehyde selectivity.

Besides catalyst activity and selectivity, the productivity of BDE is considered as a critical indicator from the standpoint of industrial development. As far as we know, the highest BDE productivities for one-pot ethanol conversion were reported by Huang et al. [31], 1.36 $g_{BDE}g_{Cat}^{-1}h^{-1}$ over Mg-SiO_2; Larina et al. [32], 0.71 $g_{BDE}g_{Cat}^{-1}h^{-1}$ over Zn-La-Zr-SiO_2 catalysts and Sushkevich and Ivanova [33], 0.58 $g_{BDE}g_{Cat}^{-1}h^{-1}$ over Ag-Promoted ZrBEA Zeolites. In this contribution, the highest BDE productivity (0.32 $g_{BDE}g_{Cat}^{-1}h^{-1}$) is achieved over the Cs-modified Zn-Zr supported catalyst while the BDE productivity on K- and Na-containing catalysts are slightly higher than that observed on the unmodified one (0.26 $g_{BDE}g_{Cat}^{-1}h^{-1}$, 0.24 $g_{BDE}g_{Cat}^{-1}h^{-1}$ and 0.23 $g_{BDE}g_{Cat}^{-1}h^{-1}$, respectively) at WHSV= 1 h^{-1} and 400 °C. Thus, the BDE productivity on Cs-promoted catalysts is significantly higher than 0.12-0.20 $g_{BDE}g_{Cat}^{-1}h^{-1}$ reported on promoted MgO/SiO_2 catalysts and 0.23 $g_{BDE}g_{Cat}^{-1}h^{-1}$ for metallic Ag-doped ZrO_2/SiO_2 catalyst under similar conditions [7, 9]. Our current productivity is also better than those observed on Hf-Zn/SiO_2 catalyst (0.17 $g_{BDE}g_{Cat}^{-1}h^{-1}$) [34], Zn-Zr/MgO-$SiO_2$ (0.17 $g_{BDE}g_{Cat}^{-1}h^{-1}$) [30] and CuTaSiBEA zeolite-based catalyst (0.12-0.19 $g_{BDE}g_{Cat}^{-1}h^{-1}$) [35]. However, it is lower than those on Na-doped $Zn_xZr_yO_x$ (0.49 $g_{BDE}g_{Cat}^{-1}h^{-1}$) [13], $ZnOMgOSiO_2$ (1.02 $g_{BDE}g_{Cat}^{-1}h^{-1}$), and $CuZrO_2ZnOSiO_2$ (0.84 $g_{BDE}g_{Cat}^{-1}h^{-1}$) [36], though lower conversion and selectivity were reported. Recently, a high productivity was reported on

Cu/MCF+Zr/MCF system (1.4 $g_{BDE}g_{Cat}^{-1}h^{-1}$) [37], though two separate reactors are required in this case.

4 Conclusions

The cooperative effect of ZnO-ZrO_2 oxides deposited over silica can considerably promote the conversion of ethanol into butadiene. Under optimised reaction conditions, a BDE of ~40% can be achieved, being the presence of both acid and base centers imperative. Although alkali metal promotion efficiently suppresses direct dehydration to ethylene, only Cs provides the appropriate balance of acid-base pairs with the suitable strength to carry out the condensation step effectively, resulting in an increased BDE yield close to 55%. Indeed, the catalytic activity and product distribution are closely related to surface acid-base properties, including nature, concentration and strength of active sites. A balanced distribution of high concentration of base and acid sites can suppress the direct dehydration reaction as well as enhance the rate of dehydrogenation, aldol condensation and MPV reactions, thus improving the production of BDE. Among the alkali metal oxides tested, Cs is the most promising promoter. The complex reaction pathway of the catalytic transformation of ethanol over supported oxide catalysts can be successfully manipulated to efficiently produce BDE.

Acknowledgements

This work was supported by the Science and Engineering Research Council (Grants 1124004031 & 1124004115) of A*STAR (Agency for Science Technology and Research), Singapore. The authors wish also to thank Mr. Ng Kang Wai Jeffrey for the technical assistance with acid-base characterisation experiments.

References

[1] A. Corma, S. Iborra, A. Velty, Chem. Rev. 107 (2007) 2411-2502.

[2] W.C. White, Chem. Biol. Interact. 166 (2007) 10-14.

[3] C. Angelici, B.M. Weckhuysen, P.C.A. Bruijnincx, ChemSusChem 6 (2013)1595-1614.

[4] E.V. Makshina, M. Dusselier, W. Janssens, J. Degreve, P.A. Jacobs, B.F. Sels, Chem Soc Rev 43 (2014) 7917-7953.

[5] C. Hamelinck, G. Hooijdonk, A. Faaij, Biomass Bioenergy 28 (2005) 384-410.

[6] W.M. Quattlebaum, W.J.Toussaint, J.T. Dunn, J. Am. Chem. Soc. 69 (1947) 593-599.

[7] E.V. Makshina, W. Janssens, B.F. Sels, P.A. Jacobs, Catal. Today 198 (2012) 338-344.

[8] G.O. Ezinkwo, V.F. Tretjakov, R.M. Talyshinky, A.M. Ilolov, T.A. Mutombo, Catal. Comm., 43 (2014) 207-212.

[9] V.L. Sushkevich, I.I. Ivanova, V.V. Ordomsky, E. Taarning, ChemSusChem 7 (2014) 2527-2536.

[10] W. Janssens, E.V. Makshina, P. Vanelderen, F. De Clippel, K. Houthoofd, S. Kerkhofs, J.A. Martens, P.A. Jacobs, B.F. Sels, ChemSusChem 8 (2015) 994-1008.

[11] C. Angelici, M.E.Z. Velthoen, B.M. Weckhuysen, P.C.A. Bruijnincx, Catal. Sci. Technol. 5 (2015) 2869-2879.

[12] Z. Han, X. Li, M. Zhang, Z. Liu, M. Gao, RSC Adv., 5 (2015) 103982-103988.

[13] R.A.L. Baylon, J. Sun, Y. Wang, Catal. Today 259 (2016) 446-452.

[14] G. Pomalaza, M. Capron, V. Ordomsky and F. Dumeigni, Catalysts, 6 (2016) 203.

[15] M.D. Jones, C.G. Keir, C. Di Iulio, R.A.M. Robertson, C.V. Williams, D.C. Apperley, Catal. Sci. Technol. 1 (2011) 267-272.

[16] M. D. Jones, Chem. Cent. J. 8 (2014) 53-57.

[17] O.V. Larina, P.I. Kyriienko, S.O. Soloviev, Theor. Exp. Chem., 51 (2015) 252-258.

[18] M. Leon, E. Diaz, S. Ordonez Catal. Today 164 (2011) 436-442.

[19] A. Corma, V. Fornes, M. T. Navarro, J. Perez-Pariente, J. Catal. 148 (1994) 569–574.

[20] C.A. Emeis, J. Catal., 141 (1993) 347-354.

[21] Vitaly L. Sushkevich, Irina I. Ivanova and Esben Taarning, Green Chem., 17 (2015) 2552–2559.

[22] V.A. Ivanov, J. Bachelier, F. Audry, J.C. Lavelley, J. Mol. Catal. A: Chem., 91 (1994) 45-59.

[23] S.H. Liu, G.K. Chuah, S. Jaenicke, J. Mol. Catal. A: Chem., 220 (2004) 267-274.

[24] J.I. Di Cosimo, V.K. Diez, M. Xu, E. Iglesia, C.R. Apesteguia, J. Catal., 178 (1998) 499-510.

[25] A.I. Biaglow, J. Šepa, R.J. Gorte, D. White, J. Catal., 151 (1995) 373-384.

[26] D. Tichit, D. Lutica, B. Coq, R. Durand, R. Teissier, J. Catal., 219 (2003) 167-175.

[27] W. Ji, Y. Chen, H.H. Kung, Appl. Catal. A: Gen., 161 (1997) 93-104.

[28] Z.D. Yong, S. Hanspal, R.J. Davis, ACS Catal., 6 (2016) 3193-3202.

[29] A. Corma, M.E. Domine, L. Nemeth, S. Valencia, J. Am. Chem. Soc., 124 (2002) 3194-3195.

[30] S. Da Ros, M.D. Jones, D. Mattia, J.C. Pinto, M. Schwaab, F.B. Noronha, S.A. Kondrat, T.C. Clarke, S.H. Taylor, ChemCatChem 2016, 8, 2376-2386.

[31] X. Huang, Y. Men, J. Wang, W. An, Y. Wang, Catal. Sic. Tech., 7 (2017) 168-180.

[32] O. V. Larina, P. I. Kyriienko, and S. O. Soloviev, Theoretical & Experimental Chem., 52 (2016) 51-56.

[33] V. L. Sushkevich and I. Ivanova, ChemSusChem, 9 (2016) 2216.

[34] T.D. Baerdemaeker, M. Feyen, U. Müller, B. Yilmaz, F.S. Xiao, W. Zhang, T. Yokoi, X. Bao, H. Gies, D.E. De Vos, ACS Catal., 2015, 5, 3393-3397.

[35] P.I. Kyriienko, O.V. Larina, S.O. Soloviev, S.M. Orlyk, C. Calers, S. Dzwigaj, ACS Sustainable Chem. Eng., 2017, 5, 2075-2083.

[36] H. Duan, Y. Yamada, S. Sato, Chem. Lett., 2016, 45, 1036

[37] J.L. Cheong, Y. Shao, S.J.R. Tan, X. Li, Y. Zhang, S.S. Lee, ACS Sustainable Chem. Eng., 2016, 4, 4887-4894.

Table and Figure Captions

Table 1. Textural and acid properties of the catalysts.

Table 2. Concentration of Brønsted (B) and Lewis (L) acid sites determined from pyridine adsorption.

Table 3. Catalytic performance in ethanol conversion over various SiO_2 supported catalysts

Table 4a. Effect of different alkali metal promoters with equal weight % on the performance of ZnO-ZrO_2/SiO_2 catalysts

Table 4b. Effect of different alkali promoters with equal atomic loading on the performance of ZnO-ZrO_2/SiO_2 catalysts

Fig. 1. NH_3-TPD profiles of various catalysts: a) SiO_2, b) $1ZnO/SiO_2$, c) $5ZrO_2/SiO_2$, d) $1ZnO\text{-}5ZrO_2/SiO_2$ and e) $0.5Cs_2O\text{-}1ZnO\text{-}5ZrO_2/SiO_2$.

Fig. 2. FTIR spectra of pyridine adsorption after evacuation at 200 °C. a) SiO_2, b) $1ZnO/SiO_2$, c) $5ZrO_2/SiO_2$, d) $1ZnO\text{-}5ZrO_2/SiO_2$ and e) $1Cs_2O\text{-}1ZnO\text{-}5ZrO_2/SiO_2$.

Fig. 3. CO_2-TPD profiles of various catalysts: a) SiO_2, b) $1ZnO/SiO_2$, c) $5ZrO_2/SiO_2$, d) $1ZnO\text{-}5ZrO_2/SiO_2$ and e) $0.5Cs_2O\text{-}1ZnO\text{-}5ZrO_2/SiO_2$.

Fig. 4. SEM images of some samples (a) SiO_2; (b) $5ZrO_2/SiO_2$ and (c) $1Cs_2O\text{-}1ZnO\text{-}5ZrO_2/SiO_2$.

Fig. 5. Catalytic performance as a function of temperature over $1ZnO\text{-}5ZrO_2/SiO_2$.

Fig. 6. Relationship between surface acid-base properties and BDE yield.

Table 1. Textural and acid properties of the catalysts.

Catalyst	Pore volume (cm^3/g)	BET surface area (m^2/g)	Amount of acid sites (mmol NH_3/g)		
			Weak	Moderate	Total
SiO_2	1.07	381.6	-	-	-
$1ZnO/SiO_2$	1.22	297.2	-	-	-
$5ZrO_2/SiO_2$	1.18	296.5	0.03 (227 °C)	0.08 (291 °C)	0.11
$1ZnO\text{-}5ZrO_2/SiO_2$	1.12	270.5	0.08 (234 °C)	0.14 (316 °C)	0.22
$1Cs_2O\text{-}1ZnO\text{-}5ZrO_2/SiO_2$	1.31	268.4	0.08 (240 °C)	0.12 (312 °C)	0.20

Table 2. Concentration of Brønsted (B) and Lewis (L) acid sites determined from pyridine adsorption.

Catalyst	B acid sites (μmol*g-1)	L acid sites (μmol*g-1)	B/L ratio
SiO_2	-	17.8	-
$1ZnO/SiO_2$	-	28.9	-
$5ZrO_2/SiO_2$	19.2	49.4	0.4
$1ZnO\text{-}5ZrO_2/SiO_2$	-	112.3	-
$0.5Cs_2O\text{-}1ZnO\text{-}5ZrO_2/SiO_2$	5.4	50.0	0.1

Table 3: Catalytic performance in ethanol conversion over various SiO_2 supported catalysts

Catalyst	**Ethanol Conversion (%)**	**Product Selectivity (%)**					
		Ethylene	Propylene	Butadiene	Butenes	Acetaldehyde	Others[b]
SiO_2	16.9	4.2	0	0	0	95.8	0
$1ZnO/SiO_2$	74.0	30.9	0	4.5	0	61.4	3.2
$5ZrO_2/SiO_2$	99.8	82.2	1.3	11.9	3.3	0	1.4
$1ZnO\text{-}5ZrO_2/SiO_2$	95.3	27.5	3	41.3	4.8	15.9	7.4

[a] Reaction conditions: 400 ^oC, WHSV= 1 h^{-1}.

[b] Others include diethylether, ethylacetate and some unidentified products.

Table 4a: Effect of different alkali metal promoters with equal weight % on the performance of ZnO-ZrO_2/SiO_2 catalysts

Catalyst	**Ethanol Conversion (%)**	**Product Selectivity (%)**					
		Ethylene	Propylene	Butadiene	Butenes	Acetaldehyde	Others[b]
$1ZnO\text{-}5ZrO_2/SiO_2$	95.3	27.5	3.0	41.3	4.8	15.9	7.4
$0.5Li_2O\text{-}1ZnO\text{-}5ZrO_2/SiO_2$	62.5	8.3	2.3	40.7	2.2	36.7	9.7
$0.5Na_2O\text{-}1ZnO\text{-}5ZrO_2/SiO_2$	93.5	14.8	2.9	47.3	4.1	21.9	9.0
$0.5K_2O\text{-}1ZnO\text{-}5ZrO_2/SiO_2$	90.4	13.2	2.8	45.7	4.0	25.7	8.6
$0.5Cs_2O\text{-}1ZnO\text{-}5ZrO_2/SiO_2$	97.7	14.6	3.2	55.8	5.0	16.2	5.2

[a] Reaction conditions: 400 ^oC, WHSV= 1 h^{-1}, 0.5 wt. % alkali metal oxide added for the supported catalysts.

[b] Others include diethylether, ethylacetate and some unidentified products.

Table 4b: Effect of different alkali promoters with equal atomic loading on the performance of ZnO-ZrO_2/SiO_2 catalysts

Catalyst	**Product Selectivity (%)**

	Ethanol Conversion (%)	Ethylene	Propylene	Butadiene	Butenes	Acetaldehyde	Others[b]
Li_2O-1ZnO-5ZrO_2/SiO_2	100.0	22.0	10.1	40.5	6.9	7.4	13.0
Na_2O-1ZnO-5ZrO_2/SiO_2	93.3	14.1	7.1	33.6	4.7	19.7	20.8
K_2O-1ZnO-5ZrO_2/SiO_2	85.1	13.0	7.6	34.3	4.6	20.5	19.9
Rb_2O-1ZnO-5ZrO_2/SiO_2	98.7	11.5	7.2	39.5	4.7	19.2	18.0
Cs_2O-1ZnO-5ZrO_2/SiO_2	97.7	14.6	3.2	55.8	5.0	16.2	5.2

[a] Reaction conditions: 400 °C, WHSV= 1 h^{-1}, the same mole of alkali metal oxide added for the supported catalysts..

[b] Others include diethylether, ethylacetate and some unidentified products.

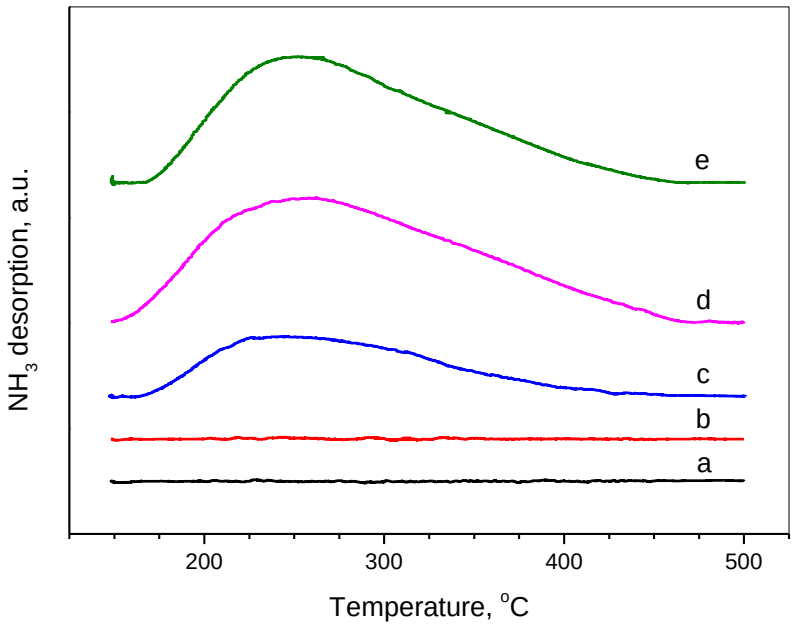

Fig. 1. NH_3-TPD profiles of various catalysts: a) SiO_2, b) $1ZnO/SiO_2$, c) $5ZrO_2/SiO_2$, d) $1ZnO\text{-}5ZrO_2/SiO_2$ and e) $0.5Cs_2O\text{-}1ZnO\text{-}5ZrO_2/SiO_2$.

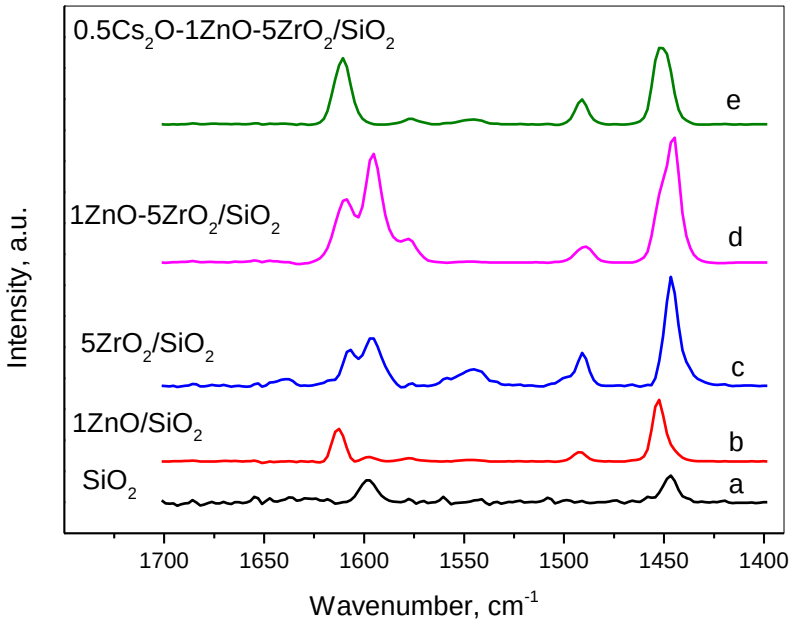

Fig. 2. FTIR spectra of pyridine adsorption after evacuation at 200 °C. a) SiO_2, b) $1ZnO/SiO_2$, c) $5ZrO_2/SiO_2$, d) $1ZnO\text{-}5ZrO_2/SiO_2$ and e) $1Cs_2O\text{-}1ZnO\text{-}5ZrO_2/SiO_2$.

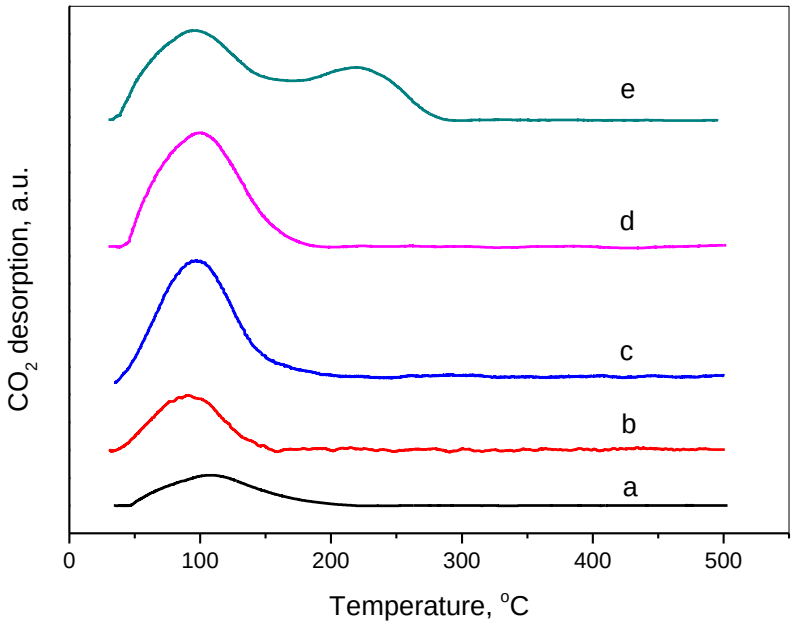

Fig. 3. CO_2-TPD profiles of various catalysts: a) SiO_2, b) $1ZnO/SiO_2$, c) $5ZrO_2/SiO_2$, d) $1ZnO\text{-}5ZrO_2/SiO_2$ and e) $0.5Cs_2O\text{-}1ZnO\text{-}5ZrO_2/SiO_2$.

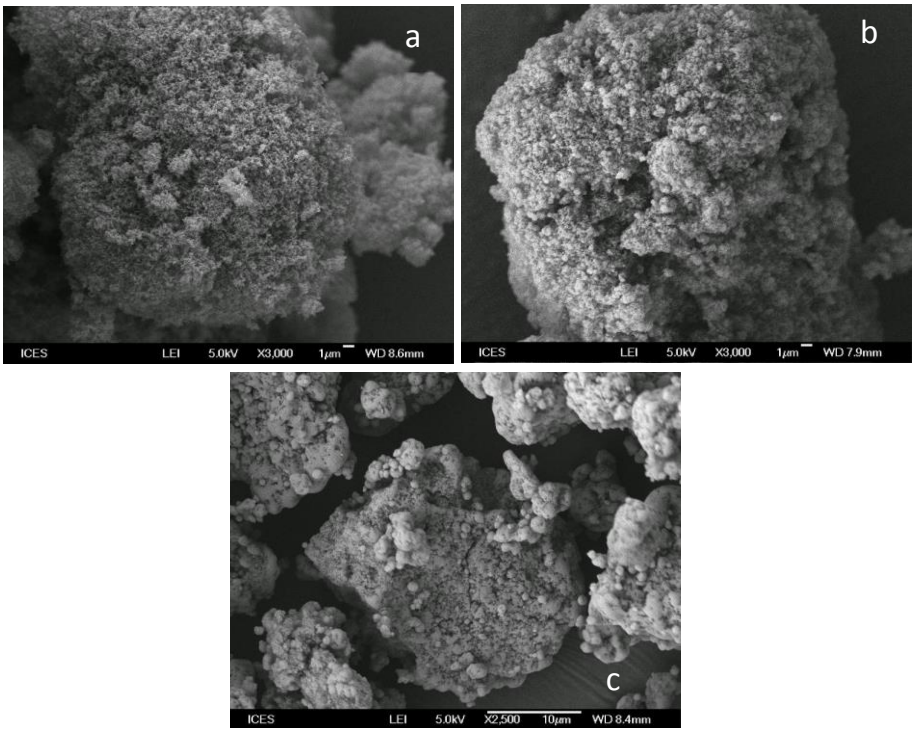

Fig. 4. SEM images of some samples (a) SiO_2; (b) $5ZrO_2/SiO_2$ and (c) $1Cs_2O$-$1ZnO$-$5ZrO_2/SiO_2$.

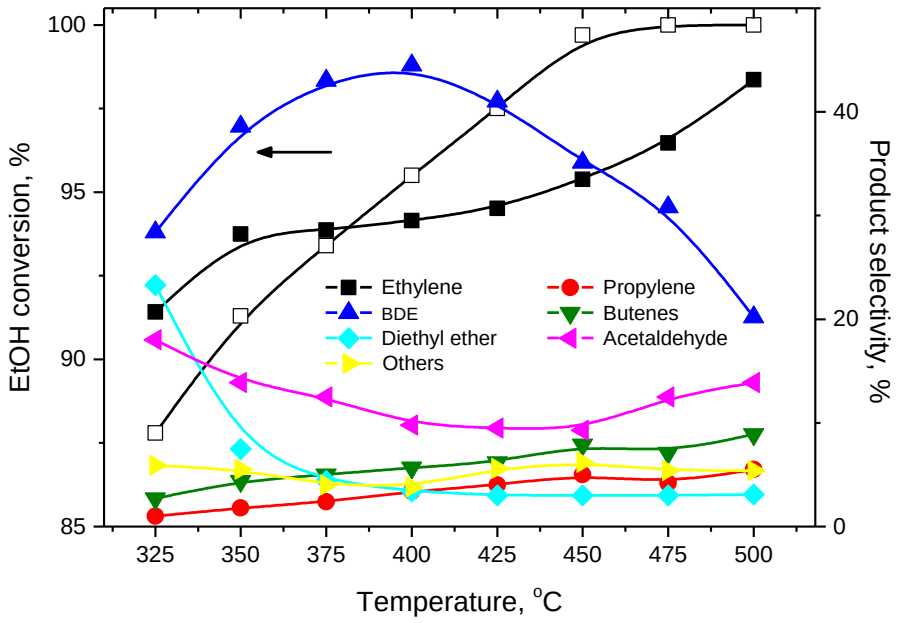

Fig. 5. Catalytic performance as a function of temperature over 1ZnO-5ZrO_2/SiO_2.

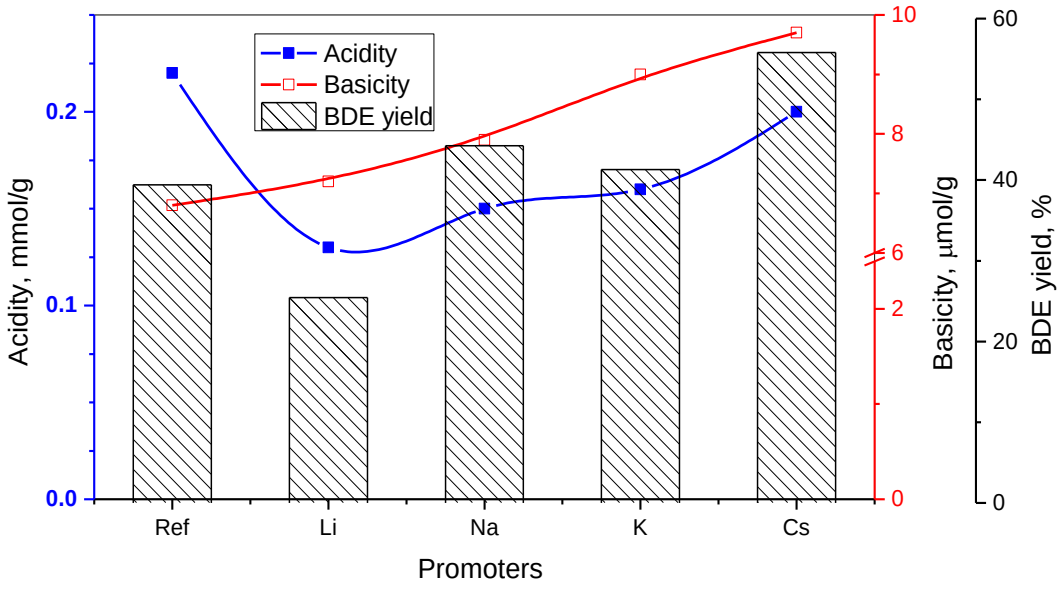

Fig. 6. Relationship between surface acid-base properties and BDE yield.

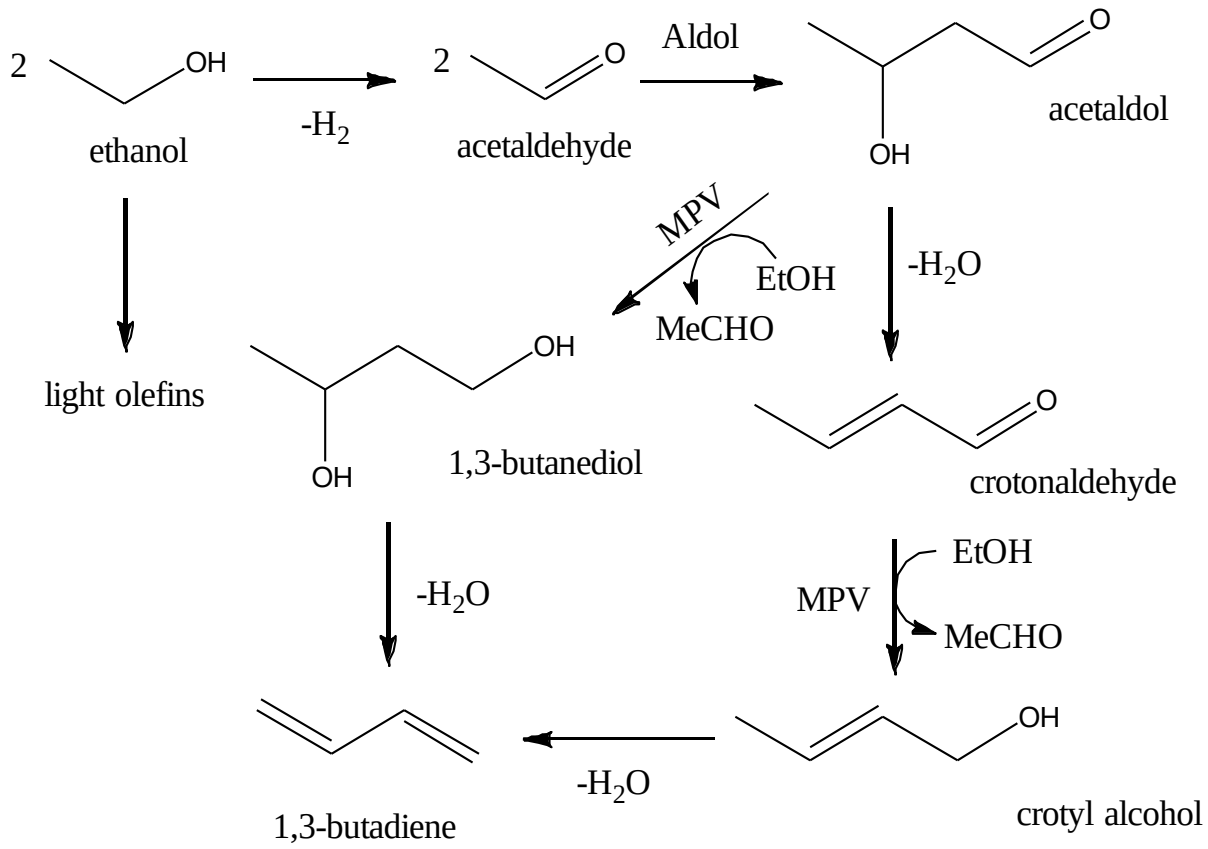

Scheme 1. Reaction pathway during butadiene formation from ethanol adapted from Jones et al. [15].